ISSN 0915-633X

NATIONAL INSTITUTE FOR FUSION SCIENCE

Flexibility of LHD Configuration with Multi-Layer Helical Coils

K. Ichiguchi, O. Motojima, K. Yamazaki,
N. Nakajima and M. Okamoto

(Received - Oct. 5, 1995)

NIFS-383 Nov. 1995

RESEARCH REPORT
NIFS Series

NAGOYA, JAPAN

Flexibility of LHD Configuration with Multi-Layer Helical Coils

Katsuji Ichiguchi, Osamu Motojima, Kozo Yamazaki,
Noriyoshi Nakajima, Masao Okamoto
National Institute for Fusion Science,
Nagoya 464-01, Japan

Abstract

The Large Helical Device (LHD) is a heliotron device with two helical coils, each of which has a structure of three current layers. It is designed so that the current in each layer should be controlled independently. By changing the combination of the coil current in the layers, it is possible to vary the effective minor radius of the helical coils, which enlarges the flexibility of the configuration. The properties of the plasmas for several combinations of the layers are investigated numerically. In the vacuum configuration, it is obtained that the combination of the layers corresponding to a large effective coil radius has a large outermost surface. In this case, the rotational transform decreases and the magnetic hill is reduced compared with the configuration with all three layers. The large Shafranov shift which is due to the small rotational transform enhances the magnetic well and the magnetic shear to stabilize the Mercier mode, however, it degrades the equilibrium beta limit. In the case of the combination for a small effective coil radius, the Mercier mode is destabilized, because the magnetic hill is enhanced. The effect on the bootstrap current is also studied.

Key Words :

LHD, multi-layer helical coils, heliotron, magnetic well, Mercier criterion, bootstrap current

1 Introduction

Recently, non-axisymmetric configurations have been extensively investigated because they are attractive with respect to the steady state operation and no major disruption. The Large Helical Device (LHD)[1, 2, 3, 4, 5], which is under construction in the National Institute for Fusion Science (NIFS), belongs to the category of the heliotron which is one of the typical concept of the non-axisymmetric configurations characterized by the continuous helical coils with a planer axis. The LHD magnetic coil system is composed of two helical coils and three pairs of poloidal field coils. Furthermore, the helical coil is composed of three layers. All coils are made from super-conducting material so that the steady state operation should be achieved. Since the continuous coils are employed, the LHD configuration has large flexibility in the operation by changing the current flowing in each component of the coils.

In the so-called standard configuration of the LHD, the electric power is supplied to all three layers in the helical coils and the total amount of the current flowing in each helical coil is the same as each other. The currents in the poloidal field coils are optimized so that the configuration should have the properties of good confinement of high energy particles, high beta limit with respect to the MHD equilibrium and stability and sufficient space for the divertor action. In this case, the major radius (R_0) and the minor radius (a_c) of the helical coils are 3.9m and 0.975m respectively, and the magnetic field strength (B_0) is 3T at $R = R_0$, where (R, ϕ, Z) denotes the cylindrical coordinate system with ϕ corresponding to the toroidal angle. The position of the magnetic axis of the vacuum magnetic surface is $R = 3.75m$, and the averaged shape of the outermost surface in the toroidal direction is almost circular. The leakage magnetic field from the coil system is also minimized simultaneously.

The parameter space of the freedom in the LHD configuration spreads around the standard configuration. Since the LHD has three pairs of the poloidal field coils, we can change the dipole, the quadrupole and the hexapole components independently. We can control the horizontal position of the plasma column by changing the dipole field. When we shift the plasma column outward in the major radius direction by the dipole field, the magnetic

well is enhanced and the magnetohydrodynamic (MHD) stability against the interchange mode becomes favorable[6]. However, the orbit loss of the deeply trapped particle[7] and the bootstrap current in the $1/\nu$ regime based on the neoclassical transport[8] are enhanced. In the case of the inward shift of the plasma column, the magnetic well is reduced and the MHD stability is degraded, however, the orbit loss and the bootstrap current are reduced. The control of the quadrupole field can be used to change the direction of the elongation (vertical or horizontal) of the averaged plasma shape in the toroidal direction. There is an optimum quadrupole field with which the shape is a little elongated horizontally in the view of the MHD stability[9]. The bootstrap current is enhanced when the shape is elongated horizontally while it is reduced when the shape is elongated vertically[8]. The orbit loss of the particle is most reduced in the case that the averaged shape is almost circular[7]. The change of the hexapole field brings the triangularity of the average shape of the plasma. For the equilibria with the fairly peaked pressure profile, the D-type shape is favorable for the enhance of the magnetic well, while the inverse D-type shape is unfavorable[10]. If we change the ratio of the currents in the helical coils, the spatial axis configuration can be generated. In this case, the minor radius of the outermost surface is reduced. The area of the magnetic hill region decreases, therefore, the fraction of the region with the magnetic well increases. However, the contribution of this effect to the MHD stability is not so significant in LHD[11].

In this paper, we focus on another flexibility in the parameter of the minor radius of the helical coils. The LHD is designed so that each layer in the helical coils can be controlled independently. All three layers are used in the standard configuration, while the operation with any combination of the layers can be carried out. By changing the combination of the layers, it is possible to change the minor radius of the helical coil effectively. For example, the coil minor radius increases if the electric power is supplied only to the outer layer in an operation, while it decreases if the power is supplied only to the inner layer. Here, the effects of the change in the coil minor radius due to the choice of the layers on the properties of the plasma are investigated. In Section 2, the structure of the helical coil is illustrated and the properties of the vacuum magnetic configurations with various coil radii are presented. The MHD properties and the bootstrap current evaluated based on the neoclassical transport theory are discussed in Sections 3 and 4, respectively. Conclusion is

given in Section 5.

2 Coil layers and vacuum configurations

Each helical coil of the LHD is composed of three layers which are called the outer (O) , the mid (M) and the inner (I) layers, as illustrated in Fig.1. The coils are designed so that the electric power can be supplied to each layer independently. Therefore, the effective minor radius of the helical coils is changed according to the choice of the combination of the layers. Hereafter, we use the pitch parameter of the helical coils defined by

$$\gamma_c \equiv \frac{m}{\ell}\frac{a_c}{R_0}, \tag{2.1}$$

which is widely utilized in designing heliotron devices. Here m and ℓ denote the number of period and the pole number of the helical coils, respectively. Since we are restricted to the LHD configurations in this paper, changing the combination of the layers corresponds to varying the parameter γ_c through the effective minor radius a_c.

In order to study the effect of the variation of γ_c, we have chosen five kinds of the combination of the layers in the LHD device, which are summarized in Table 1. The standard configuration corresponds to $\gamma_c = 1.25$. In this case, all three layers are used for generating the confinement magnetic field. If only the O-layer is used, the radius of the helical coil becomes large and γ_c increases to 1.38. On the other hand, γ_c decreases to 1.12 in the case of only the I-layer. The maximum current which can flow in each layer is limited by the property of the superconducting material. When only one layer is used, therefore, the magnetic strength is about 1/3 of that in the standard configuration as shown in Fig.2.

At first, we calculate the vacuum magnetic configurations corresponding to the combinations of the layers in Table 1. In the calculation for each configuration, the same ratios of the currents between the poloidal field coils as those of the standard configuration are used, while the total amount of the currents of all the poloidal field coils is adjusted so that the position of the magnetic axis should be located at $R = 3.75$m. Figure 3 shows the Poincaré plots of the vacuum magnetic field lines in the cases of $\gamma_c = 1.12$, 1.25 and 1.38, which are calculated under the consideration of the actual coil shape of the LHD. We determined the outermost surface by plotting only the field lines which remain in the

calculation area after the trace of 40 turns of the torus. From this figure, it is seen that the average radius of the outermost surface increases as γ_c becomes large. The relation of the averaged radius with γ_c is shown in Fig.4.

Figure 5 shows the profiles of the rotational transform for the five combinations of the layers. The reduction of the rotational transform due to the increase in γ_c is seen in this figure. The average distance between the magnetic surface with the same minor radius and the helical coils becomes large, when γ_c increases. Hence, the poloidal component of the magnetic field generated by the helical coils decreases at the magnetic surface as γ_c increases, while the averaged toroidal component of the magnetic field at the magnetic surfaces does not strongly depend on the coil radius. Therefore, the increase in γ_c results in the decrease in the rotational transform.

The magnetic well depths of the five combinations of the layers are shown in Fig.6. The well depth is defined by

$$(well\ \ depth) = \frac{V'(0) - V'(\Phi)}{V'(0)}, \tag{2.2}$$

where V denotes the volume encircled by the magnetic surface and Φ is the normalized toroidal magnetic flux inside the volume. The prime denotes the derivative with respect to Φ. In Fig.6, therefore, the region with the positive gradient of the curve of the well depth corresponds to the magnetic well region with $V'' < 0$. In the standard configuration with $\gamma_c = 1.25$, the magnetic hill spreads in the whole region inside the outermost surface. The magnetic hill is reduced as γ_c increases, and very shallow magnetic well appears in the vicinity of the magnetic axis in the case of $\gamma_c = 1.38$. On the other hand, the magnetic hill is enhanced when γ_c becomes small. This tendency can be roughly explained by using the single-harmonic approximation in the magnetic field. Under this approximation, the derivative of the specific volume can be written by[12]

$$V''(\Phi) = \frac{m}{B_0^2 \ell R} \frac{1}{r^3} \frac{d}{dr}(r^4 \iota), \tag{2.3}$$

where B_0 denotes the uniform toroidal field and r is the average radius of the flux surface. Here the rotational transform can be also approximated by

$$\iota = \iota_0 + (\iota_a - \iota_0) r^2, \tag{2.4}$$

where ι_0 and ι_a mean the rotational tranforms at the magnetic axis and the outermost surface, respectively. By substituting eq.(2.4) into eq.(2.3), we can roughly say that the

configuration with a large rotational transform has large positive V'' in the vicinity of the magnetic axis. Therefore, the configuration with γ_c=1.12 is more unfavorable than the standard configuration with respect to the magnetic well due to the large rotational transform.

If it is assumed that the longitudinal adiabatic invariance is preserved in the particle motion, the orbit of the particles deeply trapped in the helical magnetic ripples, of which the parallel velocity component to the magnetic field is very small, traces the line of the minimum of the magnetic field. Hence, the confinement of such deeply trapped particles can be simply estimated by plotting the contour of the $B_{min} \equiv \min_\phi |B|$[13]. Figure 7 shows the B_{min} contour inside the outermost magnetic surface averaged in the toroidal direction in the case of $\gamma_c = 1.38$. The contours are shifted to the inward of the torus comparing with the averaged magnetic surfaces. Thus, the contours of the B_{min} in the shaded region cannot be closed inside the outermost surface. This means that the deeply trapped particles near the outermost surface in the outward of the torus will be lost from the outermost surface. The fraction of the confinement region of the deeply trapped particles in the outermost surface is plotted in Fig.8. The dependence of the fraction on γ_c is weak compared with the case of the shift of the plasma column by controlling the vertical field[7]. The deeply trapped particles in about 80% region inside the outermost surface will be confined in the range of $1.12 \leq \gamma_c \leq 1.38$.

3 Dependence of equilibrium properties on the combination of the layers

The three-dimensional MHD equilibria for each combination of the layers in the helical coils are investigated with the VMEC code[14] under the fixed boundary condition. In this study, the currentless constraint is imposed and the pressure profile of $P = P_0(1-\Phi)^2$ is assumed. In this case, the average beta value is about 1/3 of the beta value at the magnetic axis, β_0.

Figure 9 shows the Shafranov shift of the magnetic axis, δ, defined by

$$\delta = (R_{ax} - R_{cnt})/r_{av}, \tag{3.1}$$

where R_{ax} and R_{cnt} denote the major radii of the magnetic axis and the center of the outermost surface, respectively, and r_{av} means the minor radius of the plasma. The shift in the case of $\gamma_c = 1.38$ (only O-layer) is larger than that in the standard case ($\gamma_c = 1.25$) due to the smaller ι_o in the vacuum configuration. It leads to the enhancement of the magnetic well as shown in Fig.10(c), which spreads from the region near the magnetic axis toward the edge as the beta value increases. However, the magnetic hill still remains in the peripheral region. On the other hand, because of the large ι_0 in the vacuum configuration in the case of $\gamma_c = 1.12$ (only I-layer), the small Shafranov shift of the axis seen in Fig.9 reduces the formation of the magnetic well at finite beta, as shown in Fig.10(a).

Figure 11 shows the profiles of the rotational transform at several beta values for the three types of the combination of the layers corresponding to $\gamma_c = 1.12$, 1.25 and 1.38. The tendency of the change of the profile due to the finite beta value is that ι_0 increases and the value at the mid region decreases, which is common in all cases. Therefore, the gradient of the rotational transform at the peripheral region becomes steep as beta increases. In the case of $\gamma_c = 1.38$, the change in the profile of the rotational transform is large because of the strong deformation of the flux surfaces. Hence, the significant effect of the shear stabilization against MHD instabilities can be expected in the peripheral region. In the case of $\gamma_c = 1.12$, the change of the rotational transform is small due to the small Shafranov shift of the flux surfaces, and therefore, the shear stabilization is weak.

Since the equilibria are assumed to be currentless, they are free from the current driven instabilities. Therefore, the pressure driven modes are crucial in the MHD stability. Here, we focus on the stability of the equilibria with the three combinations of the layers against the interchange mode by estimating the Mercier criterion. The Mercier criterion is a local stability criterion for the ideal interchange mode, which is given by[15, 16]

$$D_I < 0 \tag{3.2}$$

for stability, where

$$D_I = \frac{1}{4} - \frac{1}{\iota'^2}(D_{J\cdot B} + D_W + D_G) \tag{3.3}$$

$$D_{J\cdot B} = \iota' \left\langle \frac{(I'\mathbf{B} - \mathbf{J}) \cdot \mathbf{B}}{|\nabla\Phi|^2} \right\rangle \tag{3.4}$$

$$D_W = P' \left(V'' - P' \left\langle \frac{1}{\mathbf{B}^2} \right\rangle \right) \left\langle \frac{\mathbf{B}^2}{|\nabla\Phi|^2} \right\rangle \tag{3.5}$$

$$D_G = \left\langle \frac{\mathbf{J}\cdot\mathbf{B}}{|\nabla\Phi|^2} \right\rangle^2 - \left\langle \frac{\mathbf{B}^2}{|\nabla\Phi|^2} \right\rangle \left\langle \frac{(\mathbf{J}\cdot\mathbf{B})^2}{\mathbf{B}^2|\nabla\Phi|^2} \right\rangle. \tag{3.6}$$

Here the prime means the derivative with respect to Φ and the bracket denotes the flux average defined by

$$\langle f \rangle = \frac{d}{d\Phi} \int f dV. \tag{3.7}$$

Figure 12 shows the results of the Mercier stability for the cases of γ_c =1.12, 1.25 and 1.38. The level surfaces of D_I are also drawn inside the unstable regions, because the absolute value of D_I is considered to be related to the growth rate of low-n interchange instability. In the case of standard configuration with $\gamma_c = 1.25$, a weak unstable region is seen in the plasma column in Fig.12(b). However, the equilibria may be actually stable because the maximum of the absolute value of D_I is so small that the ideal interchange mode can be easily stabilized by kinetic effects such as the finite Larmor radius effect[6]. Above $\beta_0 = 8\%$, we have the second stability region with respect to the Mercier criterion. In the case of $\gamma_c = 1.38$, the unstable region completely disappears in the plasma. This is because the magnetic well and the magnetic shear stabilize the Mercier mode from the vicinity of the magnetic axis and from the peripheral region, respectively. On the other hand, the Mercier mode is strongly destabilized in the case of $\gamma_c = 1.12$ because both the stabilizing effects of magnetic well and the magnetic shear are reduced.

Figure 13 shows the equilibrium beta limit as a function of γ_c, which is determined by the convergence of the iteration in the VMEC code. The configuration with the larger γ_c has the smaller equilibrium limit owing to the enhancement of the Shafranov shift.

4 Bootstrap current estimated based on the Neoclassical theory

The neoclassical transport theory predicts that the bootstrap current can flow in non-axisymmetric plasmas as well as in tokamaks[17, 18]. Since the bootstrap current flows along the magnetic field line, the substantial amount of the bootstrap current plays an important role as a net toroidal current in the MHD equilibrium and stability. Hence, it is crucial to know how the bootstrap current is affected by varying γ_c.

Watanabe et.al[8] calculated the consistent bootstrap current in the LHD plasma with the three-dimensional MHD equilibria by iterating the equilibrium calculation with the VMEC code[14] and the estimation of the bootstrap current as a net toroidal current alternatively[8]. In this case, they assumed that both electrons and ions are in the $1/\nu$ collisional regime. Recently, Watanabe et.al[19] modified the method by incorporating a connection formula from the $1/\nu$ to the Pfirsch-Schlüter regime in non-axisymmetric systems. In the present study, we calculated the bootstrap current by following their method. The bootstrap current density in non-axisymmetric system, $\mathbf{J}_{bs}$, can be expressed by

$$\frac{\langle \mathbf{J}_{bs} \cdot \mathbf{B} \rangle}{2\pi} = \frac{1}{2}(L_{1e} + L_{1i})\frac{dP}{d\Phi} + (-L_{2e} + L_{2i})n\frac{dT}{d\Phi}. \tag{4.1}$$

Here we assumed that

$$T = T_e = T_i, \quad n = n_e = n_i, \tag{4.2}$$

for the temperature, T, and the density, n, where the subscripts e and i mean electron and ion, respectively. In this case, the contribution of the radial electric field to the bootstrap current vanishes because electrons and ions have the same collisionality. The bracket denotes the flux average. Factors of L_{ja} $(j = 1, 2, a = i, e)$, which are interpolated with the connection formula, are determined by effective charge of the ions, geometry of the flux surfaces and the collision frequencies of electrons and ions. The exact definitions of L_{ja} are given in [19].

We calculated the bootstrap current flowing in the LHD equilibria at $\beta_0 = 2\%$ with γ_c= 1.12, 1.25 and 1.38. The density is fixed as

$$n = 0.5 \times 10^{20}(1 - \Phi) \quad (m^{-3}). \tag{4.3}$$

The temperature profile of

$$T = T_0(1 - \Phi) \tag{4.4}$$

is common for the three cases, however, the factor of T_0 is adjusted to obtain the specified beta value. In the cases of γ_c =1.12 and 1.38, T_0 = 0.5keV corresponds to $\beta_0 = 2\%$ because the maximum magnetic field is about 1T as shown in Fig.2. In the case of $\gamma_c = 1.25$, the maximum field strength is 3T which corresponds to the standard configuration, while the operation with the magnetic field less than 3T can be also done. Thus, we calculate the two cases for B_0 = 1T with T_0=0.5keV and B_0 = 3T with T_0=4.5keV in $\gamma_c = 1.25$ case.

Figure 14 shows the profiles of the bootstrap currents, $I_{bs}(\Phi)$, which is defined by

$$I_{bs}(\Phi) = 2\pi \int d\Phi \frac{\langle \mathbf{J}_{bs} \cdot \mathbf{B} \rangle}{\langle B^2 \rangle}, \tag{4.5}$$

of the three types of γ_c = 1.12, 1.25 and 1.38 at β_0 = 2%. In the case of γ_c=1.25, the current with B_0 = 3T is more than 6 times of that with B_0 = 1T. There are two dominant factors for this result. One is the direct effect of the difference of the magnitude of the magnetic field. We can see from a dimensional analysis that I_{bs} is proportional to the magnetic field for a fixed beta value. Hence, the bootstrap current with B_0=3T should be three times larger than that of B_0 = 1T if other parameters would be the same. The other factor is due to the difference of the collisional regime corresponding to the difference of the temperature. The electrons and ions are in the $1/\nu$ regime for the plasma with T_0 = 4.5keV, while they are in the plateau regime for T_0=0.5keV. The connection formula included in eq.(4.1) has a tendency that the larger bootstrap current flows in the plasma in the $1/\nu$ regime than in the plateau regime. Thus, the bootstrap current with B_0=3T is much larger than that with B_0=1T.

It is also seen that the bootstrap current is enhanced as γ_c increases when we fix the magnetic field strength and the temperature. The difference between the currents for the three types of γ_c is attributed to the difference of the geometry. The factors of L_{ja} in eq.(4.1) depend on the geometry of the flux surfaces[19]. However, it has not been established how the factors depend on the geometry of the flux surfaces precisely in the heliotron configurations. There may be a tendency that the configuration with small aspect ratio and large Shafranov shift has large bootstrap current, because it is also obtained that the bootstrap current is enhanced as γ_c increases if we fix the beta value with the same magnitude of the magnetic field.

5 Conclusion

In the LHD design, the effective minor radius of the helical coil, and therefore γ_c, can be varied by changing the combination of the three layers in the helical coil. When the electric power is supplied only to the O–layer we can take the largest γ_c of 1.38 among all combinations of the three layers, while we can take the smallest γ_c of 1.12 when the power

is supplied only to the I–layer. In the standard configuration, all three layers are used and γ_c=1.25. Here we studied the effects of varying γ_c on the properties of the LHD plasma.

Two important properties drastically change according to γ_c. One is the change in the plasma radius. It is obtained that the radius of the outermost surface in the vacuum configuration increases as γ_c increases. In other words, the radius becomes the largest and the smallest when γ_c= 1.38 and 1.12, respectively. Therefore, the configuration with γ_c=1.38 is favorable in the point of having large plasma volume.

The other one is the change in the rotational transform. In the vacuum configurations, ι_0 decreases monotonically as γ_c increases. Shafranov shift of the magnetic axis due to the finite beta, which affects MHD properties through the deformation of the flux surfaces, is proportional to ι_0^{-2} in the large aspect ratio approximation. Therefore, the configuration with γ_c = 1.38 has the largest Shafranov shift of the magnetic axis, which leads to the enhancement of the magnetic well and the magnetic shear. Since the enhancement of these properties has a stabilizing effect against the interchange instability, the Mercier unstable region does not appear in the plasma with γ_c = 1.38 up to the equilibrium beta limit. On the other hand, the configuration with γ_c=1.12 has the inverse tendencies in the MHD properties to the case of γ_c=1.38 because of the large ι_0. As a result, the Mercier mode is destabilized strongly in the large region of the plasma. Thus, the configuration with γ_c=1.38 is also favorable with respect to the MHD stability. However, the equilibrium beta limit is reduced due to the large Shafranov shift in this case. The rotational transform could also be varied if the additional toroidal field coils would be provided. Therefore, the multi-layer helical coils can be considered to have a flexibility provided by the toroidal field coils.

We studied the confinement of the deeply trapped particles and the bootstrap current with respect to the neoclassical transport. The confinement of the deeply trapped particles is not sensitive to γ_c in the vacuum configurations, and about 80% of such particles are confined in each outermost surface. In the estimation of the bootstrap current, the strength of the magnetic field and the deformation of the flux surfaces due to the finite beta effects are essential. Here we compare the bootstrap currents at the same beta value. First we compare the results with B_0=1T and 3T in the case of γ_c=1.25. The temperature is different by nine times between them for the fixed beta value. In this case, the bootstrap currents are

reduced in the cases with B_0=1T not only due to the explicit dependence of the magnetic field on the bootstrap current but also through the change of the collisionality regime of the electrons and the ions. Furthermore, the bootstrap current in γ_c=1.38 is larger than that in $\gamma_c = 1.12$ because of the difference of the geometry of the flux surfaces. There may be a correlation between the bootstrap current and the Shafranov shift in non-axisymmetric plasmas.

In the view point of the experiments, the scan of γ_c would be the most appropriate for the MHD experiment. The drastic change of the MHD signals related to the interchange mode can be expected in the range of $1.12 \leq \gamma_c \leq 1.38$. In the configuration with a single layer, high beta plasma may be achieved easily with less input power than the standard configuration because the magnetic field is about 1T.

Acknowledgements

One of the authors (K.I.) thanks Dr.J.L.Johnson for the fruitful discussion.

References

[1] IIYOSHI,A., FUJIWARA,M., MOTOJIMA,O., OYABU,N., YAMAZAKI,K., Fusion Tech. **17** (1990) 169.

[2] IIYOSHI,A., YAMAZAKI,K., Phys. Plasmas **2** (1995) 2349.

[3] MOTOJIMA,O., AKAISHI,K., ASAO,M., FUJII,K.,FUJITA,J., HINO,T., HAMADA,Y., KANEKO,H., KITAGAWA,S., KUBOTA,Y., KURODA,T., MITO,T., MORIMOTO,S., NODA,N., OGAWA,Y., OHTAKE,I., OHYABU,N., SAGARA,A., SATOW,T., TAKAHATA,K., TAKEO,M.,TANAHASHI,S., TSUZUKI,T., YAMADA,S., YAMAMOTO,J., YAMAZAKI,K., YANAGI,N., YONEZU,H., FUJIWARA,M., IIYOSHI,A., Plasma Physics and Controlled Nuclear Fusion Research 1990, vol.3(1991) 513.

[4] MOTOJIMA,O., Fusion Tech. **26** (1994) 437.

[5] MOTOJIMA,O., OHYABU,N., KOMORI,A., NODA,N., YAMAZAKI,K., YAMADA,H., WATANABE,K.Y., INOUE,N., SUZUKI,H., KUBOTA,Y., YAMAMOTO,J., FUJIWARA,M., IIYOSHI,A., Fusion Tech. **27** (1995) 123.

[6] ICHIGUCHI,K., NAKAJIMA,N., OKAMOTO,M., NAKAMURA,Y., WAKATANI,M., Nucl. Fusion **33** (1993) 481.

[7] TODOROKI,J., J.Phys.Soc.Jpn **59** (1990) 2758.

[8] WATANABE,K., NAKAJIMA,N., OKAMOTO,M., NAKAMURA,Y., WAKATANI,M., Nucl. Fusion **32** (1992) 1499.

[9] NAKAMURA,Y., WAKATANI,M., LEBOUEF,J-N., CARRERAS,B.A., DOMINGUEZ,N., HOLMES,J.A., LYNCH,V.E., PAINTER,S.L., GARCIA,L., Fusion Tech. **19** (1991) 217.

[10] MATSUMOTO,T., NAKAMURA,Y., WAKATANI,M., J. Phys. Soc. Jpn. **62** (1993) 3904.

[11] MATSUMOTO,T., NAKAMURA,Y., WAKATANI,M., Submitted to J. Phys. Soc. Jpn.

[12] GREENE,J.M., JOHNSON,J.L., WEIMER,K.E., Plasma Phys. **8** (1966) 145.

[13] CARY,J.R., HEDRIC,C.L., TOLLIVER,J.S., Phys. Fluids **31** (1988) 1586.

[14] HIRSHMAN,S.P., VAN RIJ,W.I., MERKEL,P., Comp. Phys. Comm. **43** (1986) 143.

[15] MERCIER,C., Nucl. Fusion Suppl. Pt.2, (1962) 801.

[16] JOHNSON,J.L., GREENE,J.M., Plasma Phys. **9** (1967) 611.

[17] SHAING,K.C., HIRSHMAN,S.P., CALLEN,J.D., Phys. Fluids **29** (1986) 521.

[18] NAKAJIMA,N., OKAMOTO,M., J. Phys. Soc. Jpn. **61** (1992) 833.

[19] WATANABE,K., NAKAJIMA,N., OKAMOTO,M., YAMAZAKI,K., NAKAMURA,Y., WAKATANI,M., Nucl. Fusion **35** (1995) 335.

Table 1 : Effective minor radius, a_c, and pitch parameter, γ_c, of the helical coils for five combinations of the layers.

combination of layers	I	I,M	I,M,O	M,O	O
$a_c(m)$	0.872	0.922	0.975	1.023	1.074
γ_c	1.12	1.18	1.25	1.31	1.38

Figure Captions

Fig.1 (a)Schematic view of the poloidal cross section of the three layers and (b) exact structure of the helical coils.

Fig.2 Dependence of the magnetic field strength at the magnetic axis on γ_c.

Fig.3 Poincaré plots of the magnetic surfaces in the vacuum configurations with (a) $\gamma_c = 1.12$, (b) $\gamma_c = 1.25$ and (c) $\gamma_c = 1.38$.

Fig.4 Dependence of averaged radius of the outermost surface on γ_c.

Fig.5 Rotational transform profiles in the vacuum configurations. The numbers show the values of γ_c.

Fig.6 Magnetic well depth in the vacuum configurations. The numbers show the values of γ_c.

Fig.7 B_{min} contours(solid lines) inside the averaged outermost surface in the vacuum configuration with $\gamma_c = 1.38$. Shaded region shows loss region of the deeply trapped particles. Dashed line shows the averaged flux surface with half minor radius.

Fig.8 Dependence of the fraction of the confinement region of the deeply trapped particle on γ_c.

Fig.9 Shafranov shift for γ_c=1.12, 1.18, 1.25, 1.31 and 1.38.

Fig.10 Magnetic well depth for (a) $\gamma_c = 1.12$, (b) $\gamma_c = 1.25$ and (c) $\gamma_c = 1.38$. Solid, dashed, dot-dashed and two-dot-dashed lines show the profiles at $\beta_0 = 0\%$, 3%, 6% and 9%, respectively. $< r >$ denotes normalized average radius.

Fig.11 Rotational transform profiles for (a) $\gamma_c = 1.12$, (b) $\gamma_c = 1.25$ and (c) $\gamma_c = 1.38$. Each line corresponds to the same beta value in Fig.10.

Fig.12 Mercier unstable regions for (a) $\gamma_c = 1.12$, (b) $\gamma_c = 1.25$ and (c) $\gamma_c = 1.38$ in (β_0, ρ) plane. Shaded regions show unstable regions. Solid lines in these regions are the contours of the level surface of D_I with the difference of $\Delta D_I = 0.1$. In (c), the contours with $D_I > 4.0$ are not plotted because they are too dense. Dot-dashed line shows the boundary between magnetic well and hill regions. Dashed lines indicate the positions of rational surfaces corresponding to ι =1, 3/4, 2/3, 1/2 and 1/3 from right to left.

Fig.13 Equilibrium beta limit as a function of γ_c.

Fig.14 Bootstrap current I_{bs} for $\gamma_c = 1.12$, 1.25 and 1.38 at $\beta_0 = 2\%$. Solid and dashed lines correspond to $B_0 = 3$T and 1T, respectively.

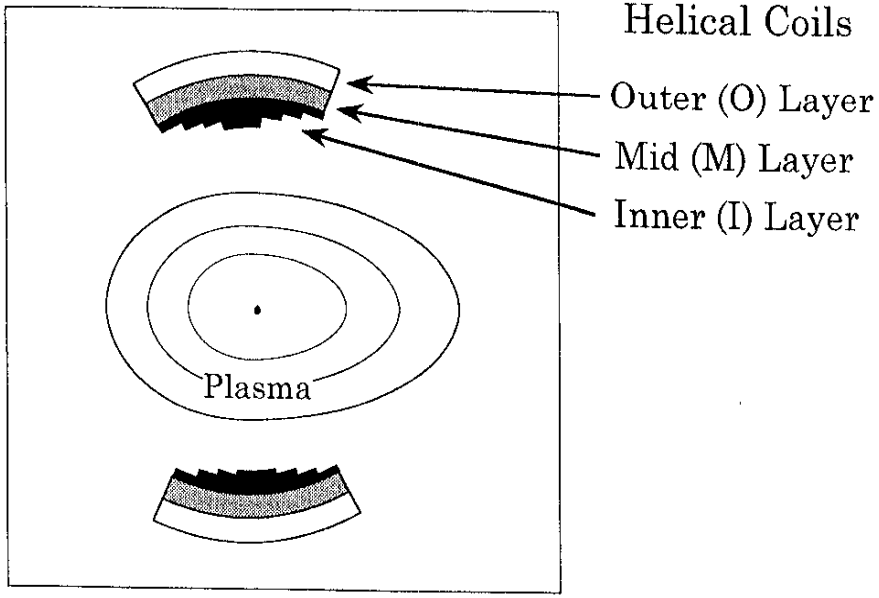
Helical Coils
Outer (O) Layer
Mid (M) Layer
Inner (I) Layer
Plasma

Fig.1 (a)

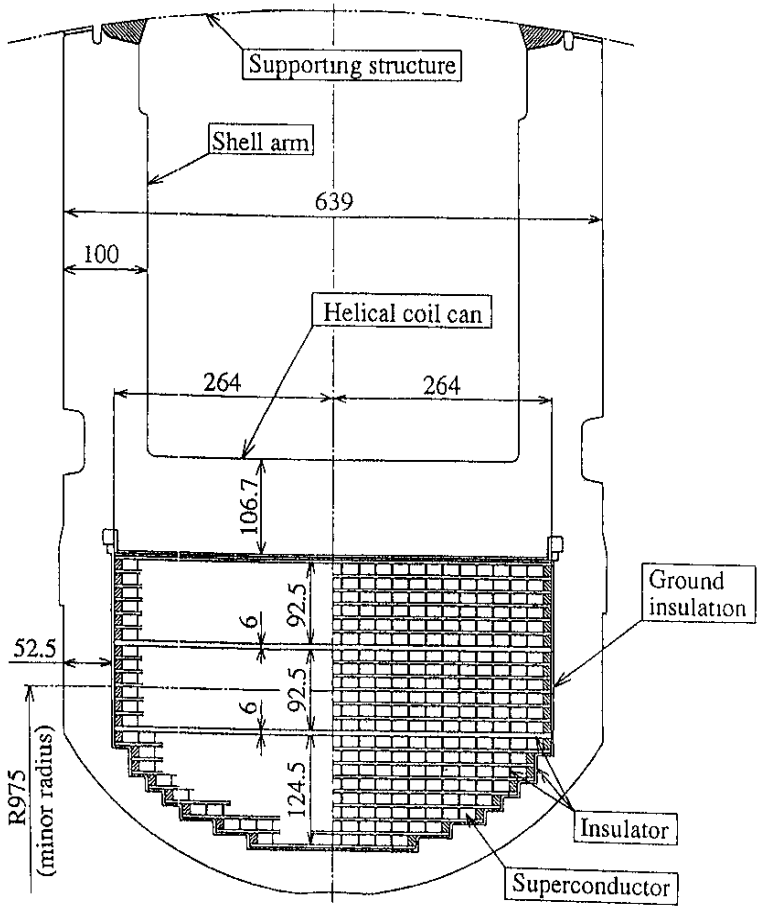
Supporting structure
Shell arm
639
100
Helical coil can
264
264
106.7
Ground insulation
92.5
6
92.5
6
124.5
52.5
R975
(minor radius)
Insulator
Superconductor

Fig.1 (b)

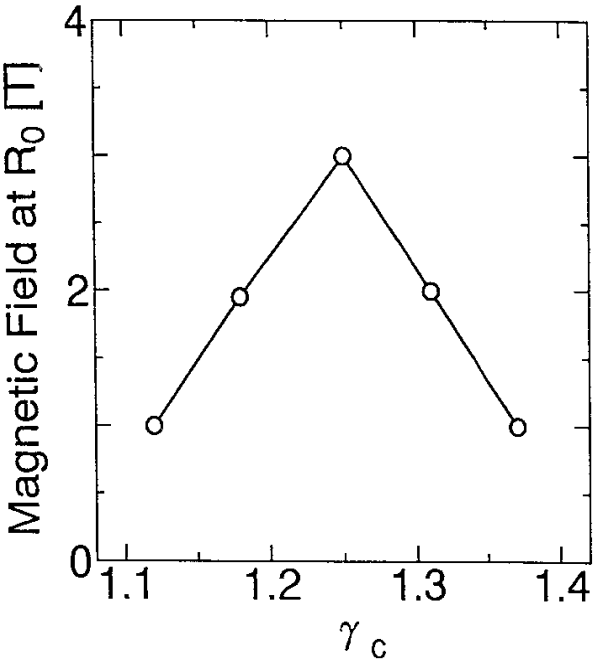

Fig.2

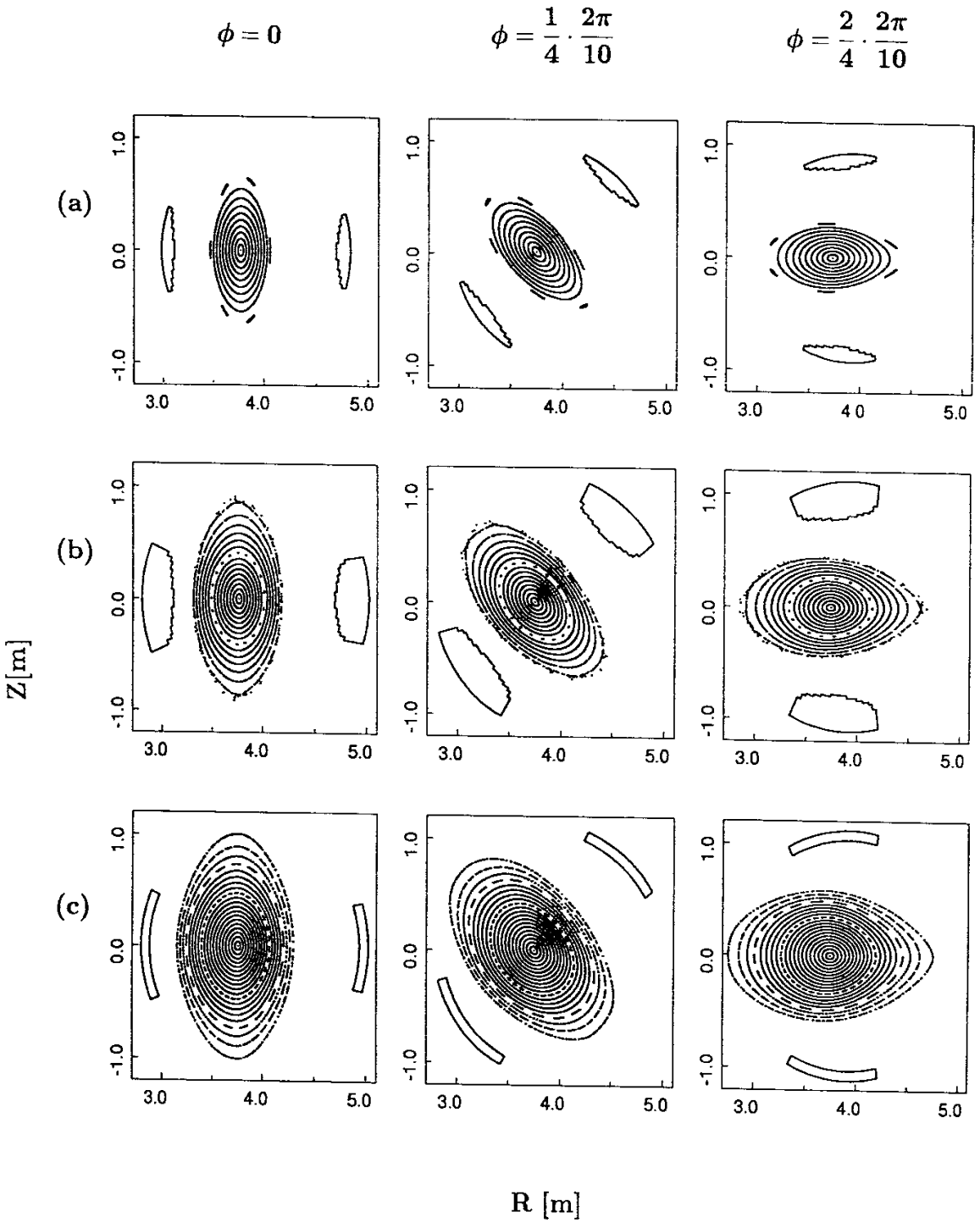
$\phi = 0$
$\phi = \frac{1}{4} \cdot \frac{2\pi}{10}$
$\phi = \frac{2}{4} \cdot \frac{2\pi}{10}$
(a)
(b)
(c)
Z[m]
R [m]
1.0
0.0
-1.0
3.0
4.0
5.0

Fig.3

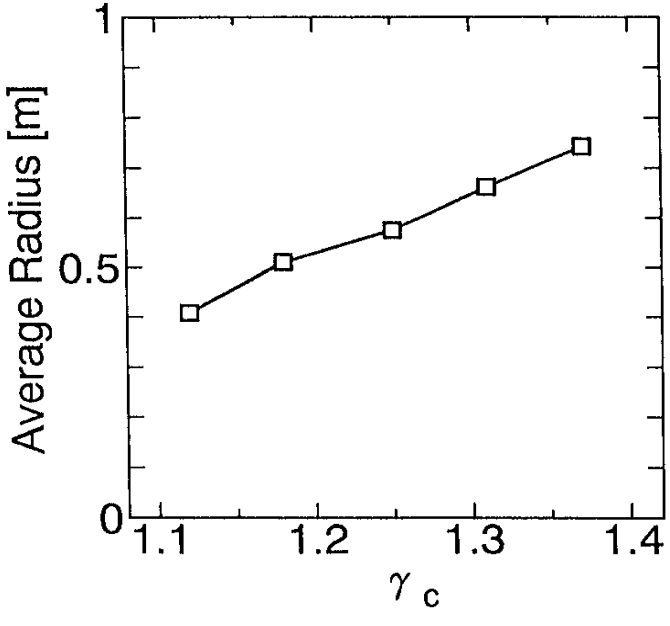
Average Radius [m]
1
0.5
0
1.1
1.2
1.3
1.4
γ_c

Fig.4

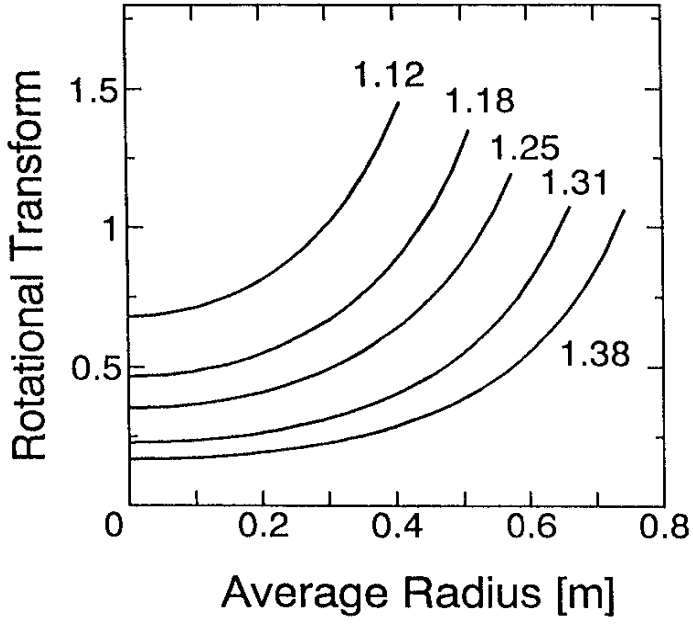
Rotational Transform
1.5
1
0.5
0
0.2
0.4
0.6
0.8
Average Radius [m]
1.12
1.18
1.25
1.31
1.38

Fig.5

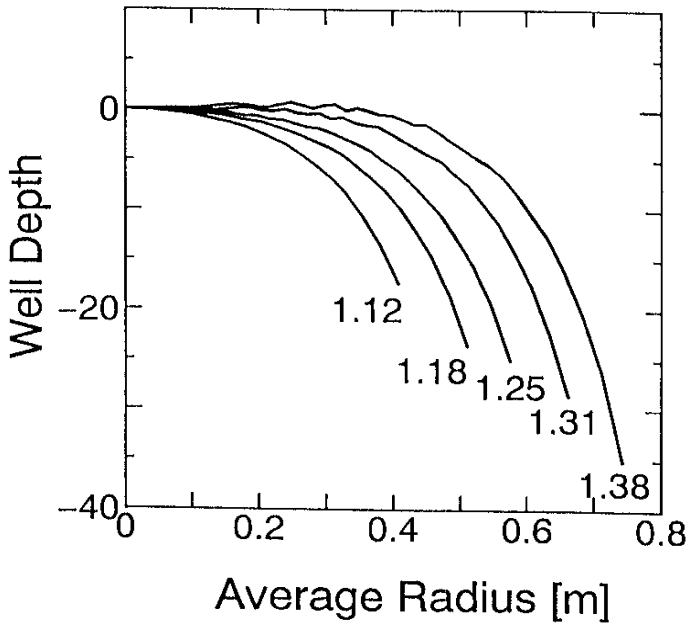
Well Depth
0
-20
-40
0
0.2
0.4
0.6
0.8
1.12
1.18
1.25
1.31
1.38
Average Radius [m]

Fig.6

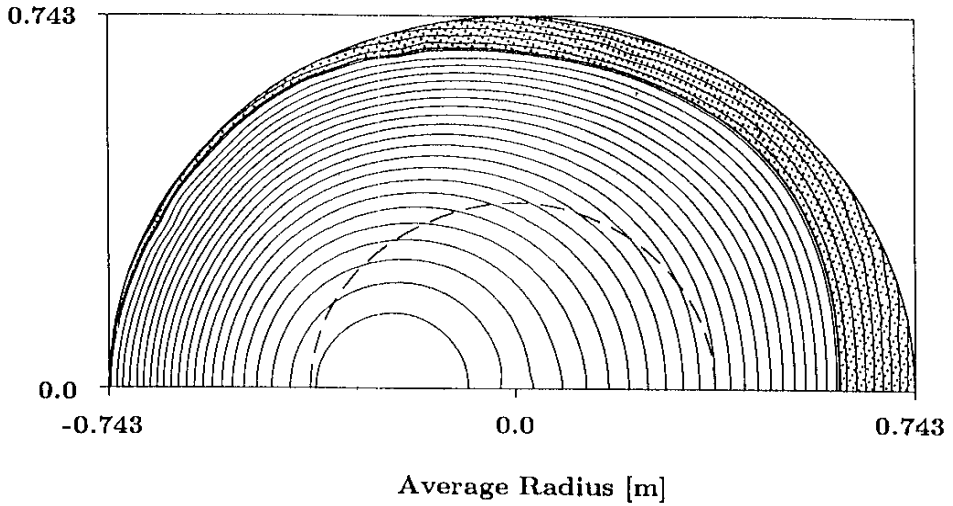
0.743
0.0
-0.743
0.0
0.743
Average Radius [m]

Fig.7

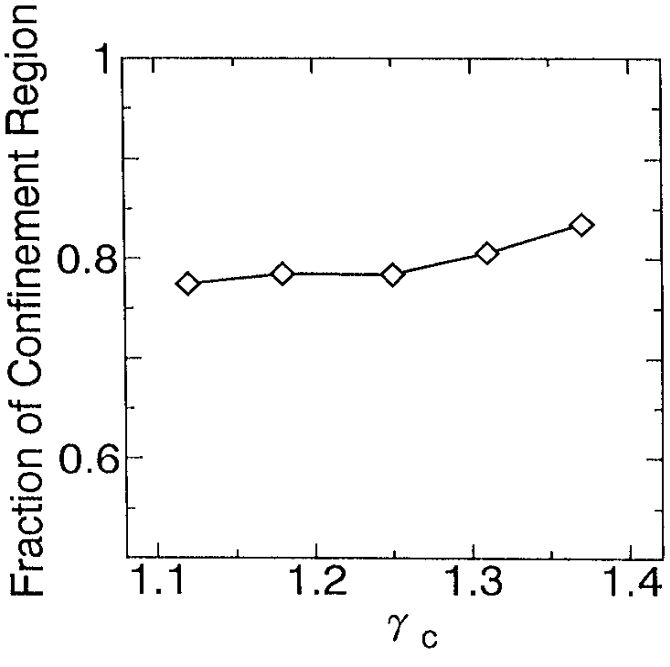
Fraction of Confinement Region
1
0.8
0.6
1.1
1.2
1.3
1.4
γ c

Fig.8

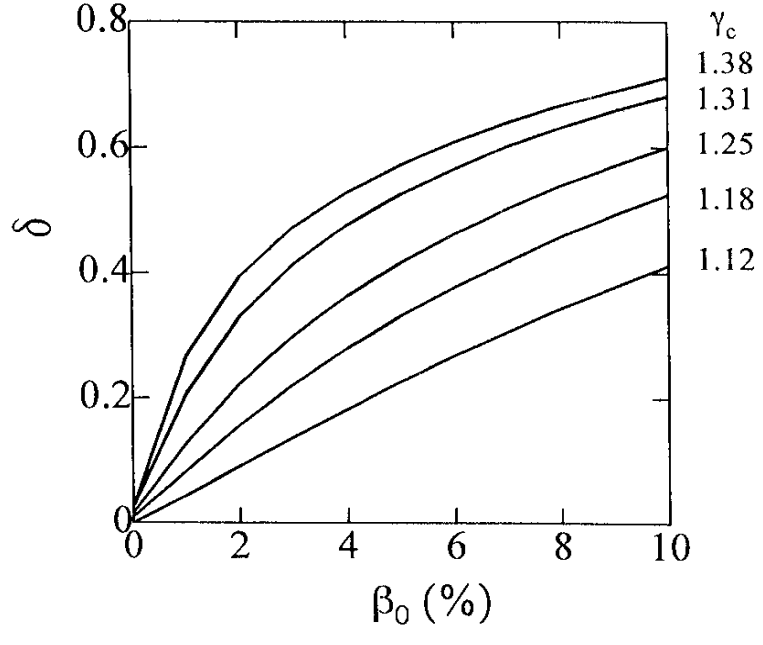
0.8
0.6
0.4
0.2
0
δ
0
2
4
6
8
10
β0 (%)
γc
1.38
1.31
1.25
1.18
1.12

Fig.9

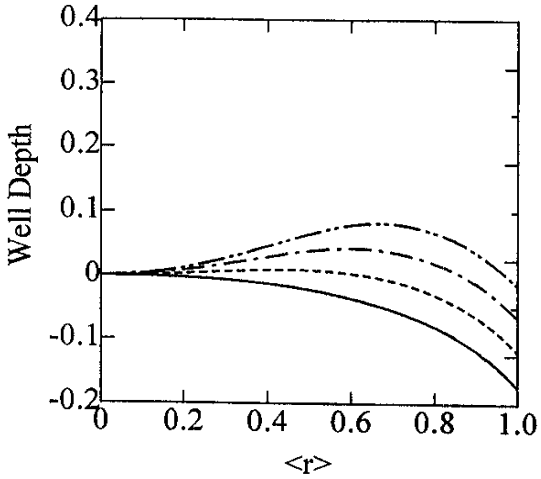

Fig.10 (a)

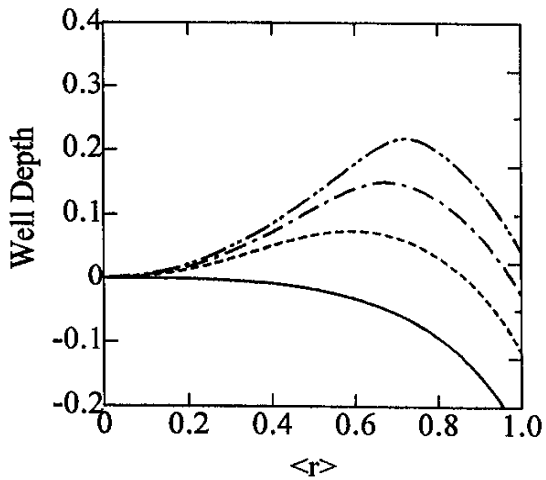

Fig.10 (b)

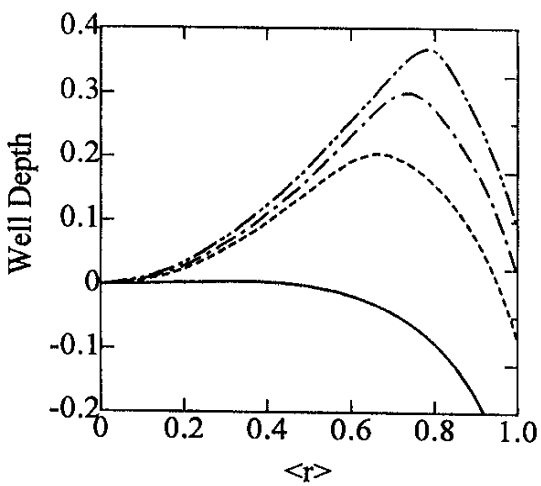

Fig.10 (c)

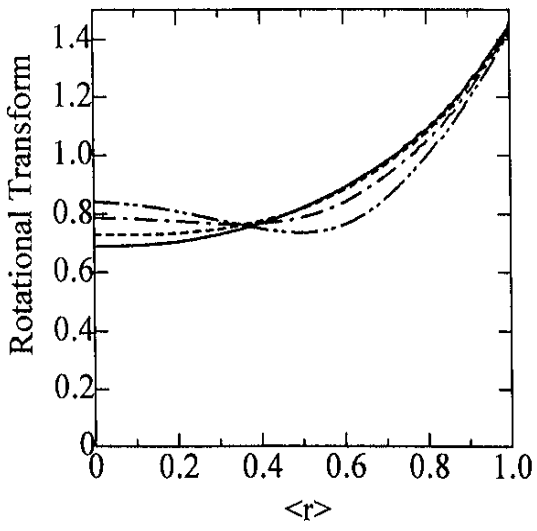

Fig.11 (a)

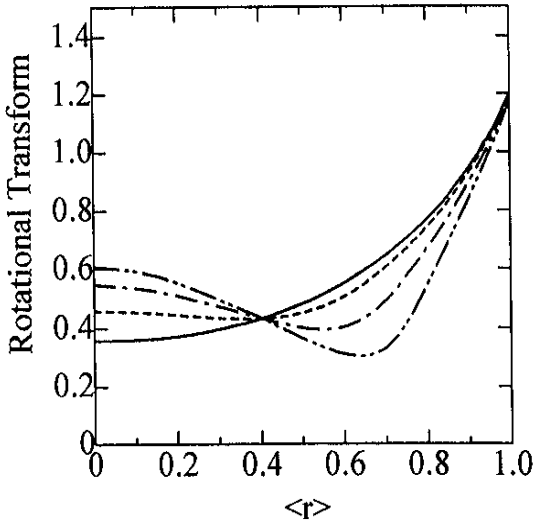

Fig.11 (b)

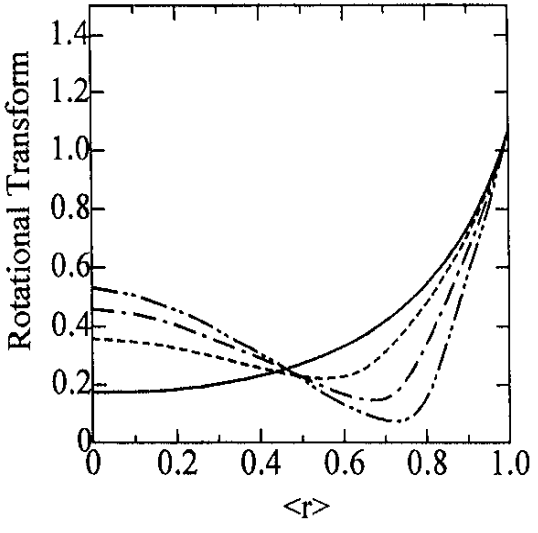

Fig.11 (c)

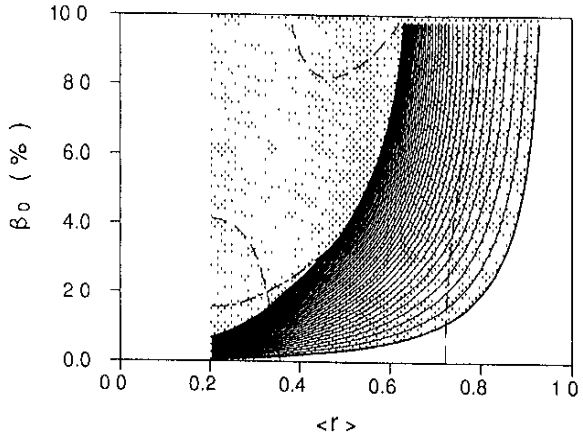

Fig.12 (a)

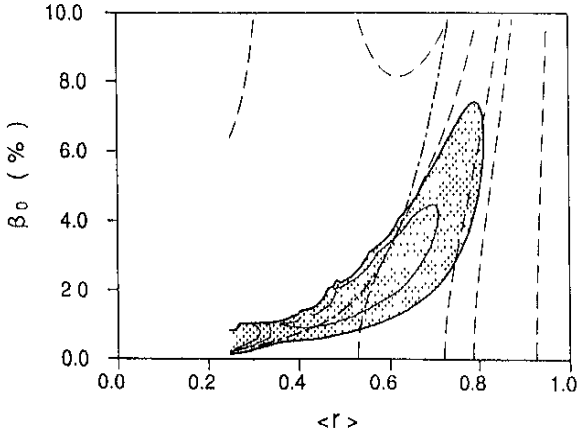

Fig.12 (b)

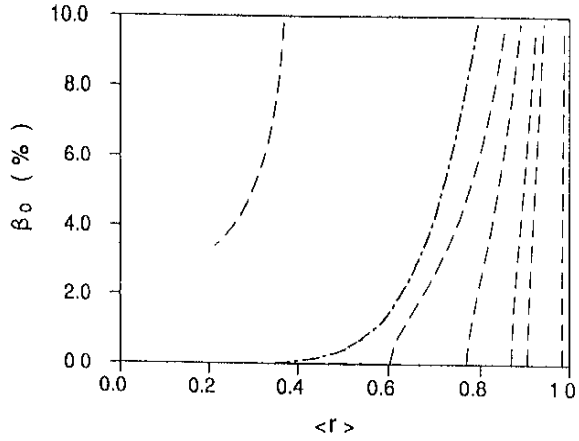

Fig.12 (c)

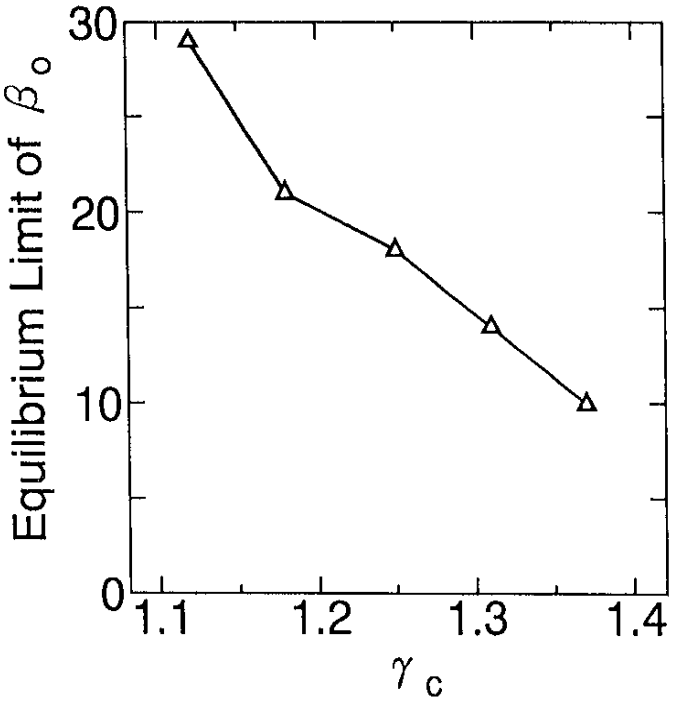
Equilibrium Limit of β_o
30
20
10
0
1.1
1.2
1.3
1.4
γ_c

Fig.13

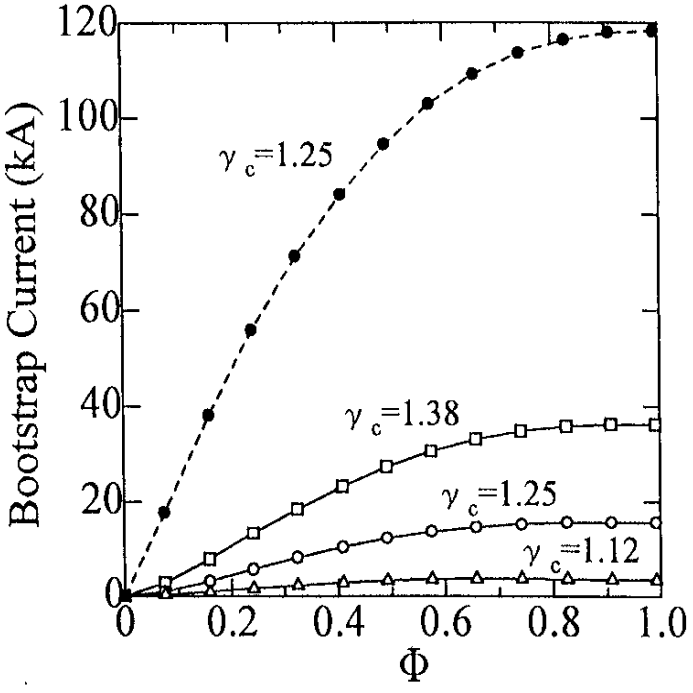
Bootstrap Current (kA)
120
100
80
60
40
20
0
0
0.2
0.4
0.6
0.8
1.0
Φ
γ_c=1.25
γ_c=1.38
γ_c=1.25
γ_c=1.12

Fig.14

Recent Issues of NIFS Series

NIFS-335 H. Takamaru, T. Sato, R. Horiuchi, K. Watanabe and Complexity Simulation Group,
A Self-Consistent Open Boundary Model for Particle Simulation in Plasmas; Feb. 1995

NIFS-336 B.B. Kadomtsev,
Quantum Telegragh : is it possible?; Feb. 1995

NIFS-337 B.B.Kadomtsev,
Ball Lightning as Self-Organization Phenomenon; Feb. 1995

NIFS-338 Y. Takeiri, A. Ando, O. Kaneko, Y. Oka, K. Tsumori, R. Akiyama, E. Asano, T. Kawamoto, M. Tanaka and T. Kuroda,
High-Energy Acceleration of an Intense Negative Ion Beam; Feb. 1995

NIFS-339 K. Toi, T. Morisaki, S. Sakakibara, S. Ohdachi, T.Minami, S. Morita, H. Yamada, K. Tanaka, K. Ida, S. Okamura, A. Ejiri, H. Iguchi, K. Nishimura, K. Matsuoka, A. Ando, J. Xu, I. Yamada, K. Narihara, R. Akiyama, H. Idei, S. Kubo, T. Ozaki, C. Takahashi, K. Tsumori,
H-Mode Study in CHS; Feb. 1995

NIFS-340 T. Okada and H. Tazawa,
Filamentation Instability in a Light Ion Beam-plasma System with External Magnetic Field; Feb. 1995

NIFS-341 T. Watanbe, G. Gnudi,
A New Algorithm for Differential-Algebraic Equations Based on HIDM; Feb. 13, 1995

NIFS-342 Y. Nejoh,
New Stationary Solutions of the Nonlinear Drift Wave Equation; Feb. 1995

NIFS-343 A. Ejiri, S. Sakakibara and K. Kawahata,
Signal Based Mixing Analysis for the Magnetohydrodynamic Mode Reconstruction from Homodyne Microwave Reflectometry; Mar.. 1995

NIFS-344 B.B.Kadomtsev, K. Itoh, S.-I. Itoh
Fast Change in Core Transport after L-H Transition; Mar. 1995

NIFS-345 W.X. Wang, M. Okamoto, N. Nakajima and S. Murakami,
An Accurate Nonlinear Monte Carlo Collision Operator; Mar. 1995

NIFS-346 S. Sasaki, S. Takamura, S. Masuzaki, S. Watanabe, T. Kato, K. Kadota,
Helium I Line Intensity Ratios in a Plasma for the Diagnostics of Fusion Edge Plasmas; Mar. 1995

NIFS-347 M. Osakabe,
Measurement of Neutron Energy on D-T Fusion Plasma Experiments; Apr. 1995

NIFS-348 M. Sita Janaki, M.R. Gupta and Brahmananda Dasgupta,
Adiabatic Electron Acceleration in a Cnoidal Wave; Apr. 1995

NIFS-349 J. Xu, K. Ida and J. Fujita,
A Note for Pitch Angle Measurement of Magnetic Field in a Toroidal Plasma Using Motional Stark Effect; Apr. 1995

NIFS-350 J. Uramoto,
Characteristics for Metal Plate Penetration of a Low Energy Negative Muonlike or Pionlike Particle Beam: Apr. 1995

NIFS-351 J. Uramoto,
An Estimation of Life Time for A Low Energy Negative Pionlike Particle Beam: Apr. 1995

NIFS-352 A. Taniike,
Energy Loss Mechanism of a Gold Ion Beam on a Tandem Acceleration System: May 1995

NIFS-353 A. Nishizawa, Y. Hamada, Y. Kawasumi and H. Iguchi,
Increase of Lifetime of Thallium Zeolite Ion Source for Single-Ended Accelerator: May 1995

NIFS-354 S. Murakami, N. Nakajima, S. Okamura and M. Okamoto,
Orbital Aspects of Reachable β Value in NBI Heated Heliotron/Torsatrons; May 1995

NIFS-355 H. Sugama and W. Horton,
Neoclassical and Anomalous Transport in Axisymmetric Toroidal Plasmas with Electrostatic Turbulence; May 1995

NIFS-356 N. Ohyabu
A New Boundary Control Scheme for Simultaneous Achievement of H-mode and Radiative Cooling (SHC Boundary); May 1995

NIFS-357 Y. Hamada, K.N. Sato, H. Sakakita, A. Nishizawa, Y. Kawasumi, R. Liang, K. Kawahata, A. Ejiri, K. Toi, K. Narihara, K. Sato, T. Seki, H. Iguchi, A. Fujisawa, K. Adachi, S. Hidekuma, S. Hirokura, K. Ida, M. Kojima, J. Koong, R. Kumazawa, H. Kuramoto, T. Minami,. M. Sasao, T. Tsuzuki, J.Xu, I. Yamada, and T. Watari,
Large Potential Change Induced by Pellet Injection in JIPP T-IIU Tokamak Plasmas; May 1995

NIFS-358 M. Ida and T. Yabe,

Implicit CIP (Cubic-Interpolated Propagation) Method in One Dimension; May 1995

NIFS-359 A. Kageyama, T. Sato and The Complexity Simulation Group,
Computer Has Solved A Historical Puzzle: Generation of Earth's Dipole Field; June 1995

NIFS-360 K. Itoh, S.-I. Itoh, M. Yagi and A. Fukuyama,
Dynamic Structure in Self-Sustained Turbulence; June 1995

NIFS-361 K. Kamada, H. Kinoshita and H. Takahashi,
Anomalous Heat Evolution of Deuteron Implanted Al on Electron Bombardment; June 1995

NIFS-362 V.D. Pustovitov,
Suppression of Pfirsch-schlüter Current by Vertical Magnetic Field in Stellarators; June 1995

NIFS-363 A. Ida, H. Sanuki and J. Todoroki
An Extended K-dV Equation for Nonlinear Magnetosonic Wave in a Multi-Ion Plasma; June 1995

NIFS-364 H. Sugama and W. Horton
Entropy Production and Onsager Symmetry in Neoclassical Transport Processes of Toroidal Plasmas; July 1995

NIFS-365 K. Itoh, S.-I. Itoh, A. Fukuyama and M. Yagi,
On the Minimum Circulating Power of Steady State Tokamaks; July 1995

NIFS-366 K. Itoh and Sanae-I. Itoh,
The Role of Electric Field in Confinement; July 1995

NIFS-367 F. Xiao and T. Yabe,
A Rational Function Based Scheme for Solving Advection Equation; July 1995

NIFS-368 Y. Takeiri, O. Kaneko, Y. Oka, K. Tsumori, E. Asano, R. Akiyama, T. Kawamoto and T. Kuroda,
Multi-Beamlet Focusing of Intense Negative Ion Beams by Aperture Displacement Technique; Aug. 1995

NIFS-369 A. Ando, Y. Takeiri, O. Kaneko, Y. Oka, K. Tsumori, E. Asano, T. Kawamoto, R. Akiyama and T. Kuroda,
Experiments of an Intense H- Ion Beam Acceleration; Aug. 1995

NIFS-370 M. Sasao, A. Taniike, I. Nomura, M. Wada, H. Yamaoka and M. Sato,
Development of Diagnostic Beams for Alpha Particle Measurement on ITER; Aug. 1995

NIFS-371 S. Yamaguchi, J. Yamamoto and O. Motojima;
A New Cable -in conduit Conductor Magnet with Insulated Strands; Sep. 1995

NIFS-372 H. Miura,
Enstrophy Generation in a Shock-Dominated Turbulence; Sep. 1995

NIFS-373 M. Natsir, A. Sagara, K. Tsuzuki, B. Tsuchiya, Y. Hasegawa, O. Motojima,
Control of Discharge Conditions to Reduce Hydrogen Content in Low Z Films Produced with DC Glow; Sep. 1995

NIFS-374 K. Tsuzuki, M. Natsir, N. Inoue, A. Sagara, N. Noda, O. Motojima, T. Mochizuki, I. Fujita, T. Hino and T. Yamashina,
Behavior of Hydrogen Atoms in Boron Films during H_2 and He Glow Discharge and Thermal Desorption; Sep. 1995

NIFS-375 U. Stroth, M. Murakami, R.A. Dory, H. Yamada, S. Okamura, F. Sano and T. Obiki,
Energy Confinement Scaling from the International Stellarator Database; Sep. 1995

NIFS-376 S. Bazdenkov, T. Sato, K. Watanabe and The Complexity Simulation Group,
Multi-Scale Semi-Ideal Magnetohydrodynamics of a Tokamak Plasma; Sep. 1995

NIFS-377 J. Uramoto,
Extraction of Negative Pionlike Particles from a H2 or D2 Gas Discharge Plasma in Magnetic Field; Sep. 1995

NIFS-378 K. Akaishi,
Theoretical Consideration for the Outgassing Characteristics of an Unbaked Vacuum System; Oct. 1995

NIFS-379 H. Shimazu, S. Machida and M. Tanaka,
Macro-Particle Simulation of Collisionless Parallel Shocks; Oct. 1995

NIFS-380 N. Kondo and Y. Kondoh,
Eigenfunction Spectrum Analysis for Self-organization in Dissipative Solitons; Oct. 1995

NIFS-381 Y. Kondoh, M. Yoshizawa, A. Nakano and T. Yabe,
Self-organization of Two-dimensional Incompressible Viscous Flow in a Friction-free Box; Oct. 1995

NIFS-382 Y.N. Nejoh and H. Sanuki,
The Effects of the Beam and Ion Temperatures on Ion-Acoustic Waves in an Electron Beam-Plasma System; Oct. 1995